Journal of Alloys and Compounds 509 (2011) 4300–4303

Contents lists available at ScienceDirect

Journal of Alloys and Compounds

journal homepage: www.elsevier.com/locate/jallcom

Theoretical study of structural, electronic, lattice dynamical and dielectric properties of $SrAl_2O_4$

Bo Liu*, Mu Gu, Xiaolin Liu, Shiming Huang, Chen Ni

Shanghai Key Laboratory of Special Artificial Microstructure Materials and Technology, Department of Physics, Tongji University, Shanghai 200092, PR China

ARTICLE INFO

Article history:
Received 11 August 2010
Received in revised form 5 January 2011
Accepted 7 January 2011
Available online 14 January 2011

Keywords:
$SrAl_2O_4$
Electronic structure
Phonon frequency
Dielectric permittivity

ABSTRACT

We investigate the structural, electronic, lattice dynamical, and dielectric properties of $SrAl_2O_4$ within density-function theory. The crystal structure is fully relaxed, and the structural parameters are found to be well consistent with the experimental data. The first pressure derivatives of the bulk modulus are predicted to be 2.5 and 4.3 for local density approximation (LDA) and generalized gradient approximation (GGA), respectively. The electronic band structure shows that the valence band maximum is comprised of O 2p states and a small amount of Al 3s and 3p states, and the conduction band minimum is comprised of Sr 5s and a small amount of O 2p, Al 3s and Al 3p states. The phonon frequencies at the center of the Brillouin zone and the dielectric permittivity tensors are calculated using density-function perturbation theory. The electronic (ε_∞) and static (ε_0) dielectric permittivity tensors are theoretically predicted by the calculations with both LDA and GGA formalisms. The results show that the electronic dielectric permittivity is isotropic, while the static dielectric permittivity exhibits to be somewhat anisotropic due to the dominant ionic contributions in static dielectric permittivity.

1. Introduction

Alkaline-earth aluminates are important luminescent host materials [1–3] due to their high quantum efficiency, excellent physical and chemical properties and the easy preparation. For instance, rare-earth ions doped $SrAl_2O_4$ as long-lasting phosphors have been extensively studied in recent years [4–7]. $SrAl_2O_4$:Eu^{2+} phosphor has also attracted considerable attention for its mechanoluminescence behavior arising from the strain field induced by the application of an external stress [8–10]. However, only a few theoretical calculations on $SrAl_2O_4$ can be found in literatures. The electronic structure of $SrAl_2O_4$ was calculated by using the scalar-relativistic full potential linearized augmented plane wave method [11]. The theoretical calculations of elastic coefficients revealed that $SrAl_2O_4$ stuffed tridymite could be a relatively soft oxide [12]. The electronic properties of $SrAl_2O_4$:Eu^{2+} were investigated by using UV–VUV synchrotron radiation spectra and density functional theory calculations, which confirmed that the electrons were the main charge carriers mostly influencing the persistent luminescence process in this material [13].

Electronic property is fundamentally critical for the luminescent properties of solids. The electronic structure of host lattice could give rise to the fundamental absorption of excitation energy which may then be transferred to the luminescent centers (i.e. rare-earth ions) resulting in effective luminescence. Furthermore, lattice vibration (phonon) can also severely affect the luminescent quantum efficiency through the nonradiative transitions of multiphonon orbit–lattice relaxation of excited states in rare-earth ions doped crystals. For instance, the effective phonon energy with 283 cm^{-1} was estimated by the study of electron-vibrational interaction in persistent phosphors $Mg_xSr_{1-x}Al_2O_4$:Eu, Dy [14]. The present work provides a thorough investigation of structural, electronic, lattice dynamical, and dielectric properties of $SrAl_2O_4$ by using first-principles calculations. We also give the analysis and comparisons of the calculated results with the experiments available in literatures.

2. Calculation details

All calculations were performed using the ABINIT package [15,16], which is based on pseudopotentials and plane-waves. Exchange and correlation were treated in the local density approximation (LDA) and generalized gradient approximation (GGA) using density-functional theory (DFT) [17,18]. It relies on an efficient fast Fourier transform algorithm for the conversion of wave functions between real and reciprocal space on the adaptation to a fixed potential of the band-by-band conjugate gradient method and on a potential-based conjugate-gradient algorithm for the determination of the self-consistent potential. The Teter parametrization fitting the Ceperley–Alder exchange-correlation data [19] was

* Corresponding author.
E-mail address: lbo@tongji.edu.cn (B. Liu).

0925-8388/$ – see front matter © 2011 Elsevier B.V. All rights reserved.
doi:10.1016/j.jallcom.2011.01.046

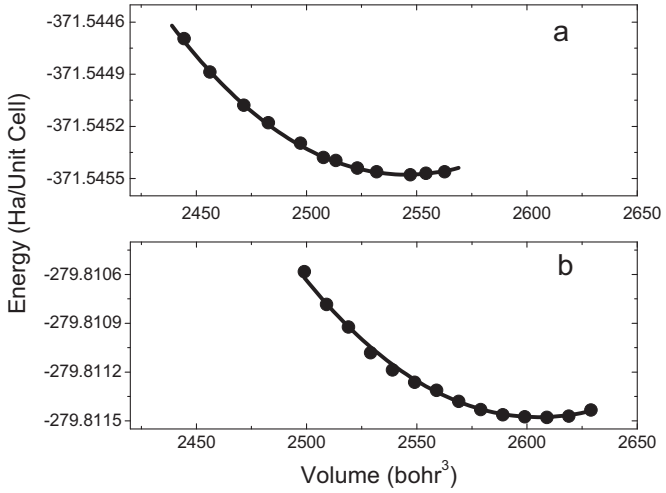

Fig. 1. Calculated total energies with LDA (a) and GGA (b) for $SrAl_2O_4$ as a function of volume. Dots represent calculated values and the solid lines are fitting results by using third-order Birch–Murnaghan equation of state.

applied for LDA calculations, and the Perdew–Burke–Ernzerhof (PBE) [20] functional was applied for GGA calculations. Relaxation of the lattice parameters and interatomic positions within the unit cell was performed using the Broyden–Fletcher–Goldfarb–Shanno algorithm [21] until the maximum component of force acting on any atoms is less than 1 mhartree/bohr.

Linear response properties were obtained as second-order derivatives of the total energy with respect to an external electric field or to atomic displacements within the framework of density functional perturbation theory (DFPT) [22,23]. The electronic wavefunctions were expanded in plane waves up to a kinetic energy cut-off of 40 Ha (1 Ha = 27.211 eV), and it was confirmed that the total energies were converged within 1 meV/atom with respect to that at 45 Ha. The Brillouin zone (BZ) was sampled by a $4 \times 4 \times 4$ Monkhorst-Pack [24] mesh of k points, with the total energies converged within 0.1 meV/atom with respect to that by a $4 \times 4 \times 8$ Monkhorst-Pack. The BZ sampling and the kinetic energy cutoff were sufficient to guarantee an excellent convergence within 1 cm^{-1} for the calculated phonon frequencies.

3. Results and discussion

3.1. Structural properties

$SrAl_2O_4$ belongs to monoclinic structure (space group $P2_1$) containing four formula units (28 atoms). All the atoms occupy 2a sites according to the Wyckoff notation. $SrAl_2O_4$ has a stuffed tridymite-like structure built up of layers of $[AlO_4]^{5-}$ tetrahedra sharing corners that give rise to six corner rings. Sr^{2+} ions are located in the cavities of the framework of $[AlO_4]^{5-}$ tetrahedra, occupying two different sites with low symmetry and coordinated by nine oxygen atoms [25].

Fig. 1 shows the calculated total energies of $SrAl_2O_4$ with LDA (a) and GGA (b) as a function of volume. The calculated equilibrium volumes (V_0), the bulk modulus (B_0) and the first pressure derivative of bulk modulus (B_0') are determined by fitting the total energy as a function of volume to the third-order Birch–Murnaghan equation of state (EOS) [26]. The results are summarized in Table 1. The calculated lattice parameters are found to be in excellent agreement with experimental data [27]. It is found that LDA underestimates the lattice parameters, while GGA overestimates them. The errors on the lattice parameters for LDA and GGA are both less than 1%. The consistency of the calculated lattice parameters with experimental

Table 1
Structure parameters of $SrAl_2O_4$.

	Exp.	LDA	GGA
a (Å)	8.447	8.412	8.482
b (Å)	8.816	8.792	8.836
c (Å)	5.163	5.132	5.203
β (°)	93.420	93.420	93.417
V (Å^3)	383.797	378.878	389.256
B (GPa)	102	90.5	112.6
B'	–	2.5	4.3

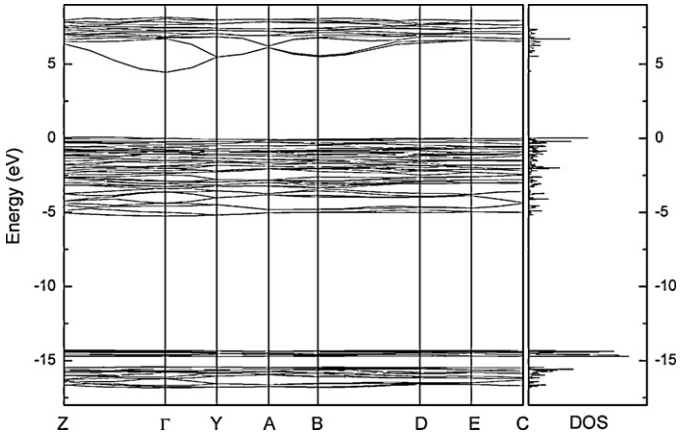

Fig. 2. Electronic band structure of $SrAl_2O_4$ calculated with LDA.

results shows that the theoretical method is valid. The calculated bulk moduli (90.5 and 112.6 GPa for LDA and GGA, respectively) are both close to the experimental value of 102 GPa [28]. The first pressure derivatives of the bulk modulus are 2.5 and 4.3 for LDA and GGA, respectively. Currently, there is no experimental value available for comparison. The large difference of B_0' for LDA and GGA is probably due to the high sensitivity for the derivative of pressure.

3.2. Electronic properties

The electronic band structure and the densities of states (DOS) of $SrAl_2O_4$ are calculated by both LDA and GGA methods. Due to the similar results of LDA and GGA, the calculated band structures and DOS profiles with LDA are presented in Figs. 2 and 3.

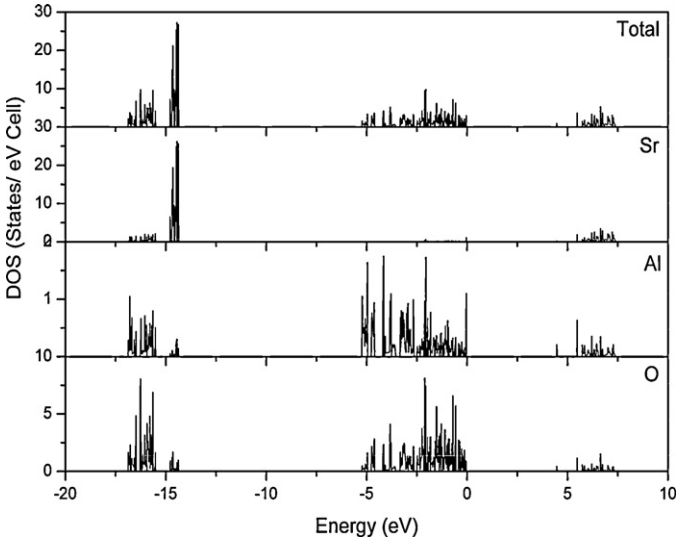

Fig. 3. Electronic density of states $SrAl_2O_4$ calculated with LDA.

Table 2
Nonvanishing components of the calculated Born effective charge tensors for $SrAl_2O_4$.

Atom	Born effective charge tensors
Sr	(2.55, 2.49, 2.51)
Sr	(2.60, 2.44, 2.40)
Al	(2.29, 2.42, 2.58)
Al	(2.49, 2.53, 2.37)
Al	(2.39, 2.38, 2.56)
Al	(2.33, 2.58, 2.40)
O	$\begin{pmatrix} -1.71 & 0.19 & 0.32 \\ 0.34 & -1.81 & -0.19 \\ 0.20 & -0.22 & -2.02 \end{pmatrix}$
O	$\begin{pmatrix} -1.72 & 0.23 & -0.28 \\ 0.02 & -1.87 & 0.25 \\ -0.30 & 0.24 & -1.91 \end{pmatrix}$
O	$\begin{pmatrix} -2.40 & -0.07 & -0.008 \\ -0.04 & -1.74 & 0.13 \\ -0.05 & 0.14 & -1.46 \end{pmatrix}$
O	$\begin{pmatrix} -2.40 & -0.07 & -0.008 \\ -0.03 & -1.41 & 0.11 \\ 0.10 & 0.01 & -1.74 \end{pmatrix}$

The calculated electronic band structure indicates that the direct band gap is located at Γ point. Most of the bands except for the three bands at the bottom of conduction band exhibit to be very flat, which is the typically character of an insulator. It is well known that the LDA and GGA usually lead to a significant underestimation of band-gap. The experimental band gap is about 6.5 eV [29]. The calculated band gaps of 4.46 eV (LDA) and 4.49 eV (GGA) are consistent with the previous result by GGA calculations [11]. From the DOS profiles in Fig. 3, it is found that in the valence band (VB) structure, the bands located at around −17 to −14 eV mainly compose of Sr 4p and O 2s states and the bands located at −5 to 0 eV compose of O 2p states and a small amount of Al 3s and 3p states. Beyond the gap, the conduction band (CB) is comprised of Sr 5s and a small amount of O 2p, Al 3s and Al 3p states.

3.3. Born effective charge tensors

The Born effective charge tensors Z^* for Sr, Al and O atoms, shown in Table 2, were calculated by perturbation theory. The form of effective charge tensor for the constituents could be determined by the site symmetry of the ions. Z^* of cations Sr and Al are almost diagonal with an anisotropy of 8% for Sr and 7% for Al. It is found that the values of Z^* of Sr are larger than its nominal ionic charge Z = +2 while the values of Z^* of Al are smaller than its nominal ionic charge Z = +3, indicating a mixed covalent–ionic bonding. The Born effective charge tensors of O ions have nonequivalent diagonal components as well as sizable off-diagonal components due to the lower symmetry.

3.4. Phonon frequencies at the Γ point

Linear response calculations were performed for the study of lattice dynamical properties. The present calculations of lattice dynamical properties were limited at the zone-center (Γ point) in BZ. The theoretical group analysis predicts the following irreducible representations of acoustical and optical zone-center modes:

$$\Gamma_{aco} = A + 2B \quad (1)$$

$$\Gamma_{opt} = 41A + 40B \quad (2)$$

For the optical modes, the modes A and B are both Raman and infrared (IR) active. The calculated phonon frequencies of $SrAl_2O_4$ with LDA and GGA at Γ point are listed in Table 3. It is evident that the phonons are very complicated since there are 81 optical phonon frequencies and the calculated results with LDA and GGA are very consistent. The experimental Raman spectrum [30] exhibits a lot of phonon frequencies in the range of 80–900 cm^{-1}. The range of calculated phonon frequencies is in accord with the experiments. However, it is not possible to give the explicit assignment and comparison because the experiment values are not obtained from orientation measurement. The calculated oscillator strengths of each phonon mode with LDA are presented in Fig. 4. It is found that the phonon at 465 cm^{-1} belonging to the bending vibration of the O–Al–O angle has the strongest oscillator strength. This could be

Table 3
Calculated phonon frequencies of $SrAl_2O_4$ at Γ point. The unit is cm^{-1}.

A modes		*B* modes	
LDA	GGA	LDA	GGA
70.0	68.1	71.6	70.9
95.5	92.3	108.9	107.6
112.2	110.2	111.0	110.3
115.2	115.6	120.8	122.3
121.1	120.3	137.6	136.3
132.0	133.2	151.1	150.3
137.6	137.3	156.1	155.3
146.4	146.6	176.4	177.3
157.1	159.3	191.4	190.3
167.4	163.2	223.7	220.3
190.1	188.3	229.3	227.3
219.2	215.1	232.8	230.3
230.6	233.2	249.9	247.6
252.6	256.3	265.4	266.3
264.9	268.3	276.0	277.3
287.0	284.3	295.9	294.3
288.9	286.3	305.5	305.3
335.9	330.3	350.7	351.3
342.9	340.3	367.6	366.3
362.8	360.0	376.2	377.3
380.5	377.3	392.8	392.3
386.2	381.3	410.0	411.3
399.7	390.0	414.8	416.3
410.6	403.3	424.1	420.3
420.6	422.3	464.0	460.3
431.5	433.3	472.6	479.3
521.0	519.3	528.9	520.3
565.1	566.3	603.4	606.3
583.5	583.1	636.1	639.3
604.4	601.0	643.3	644.3
643.3	640.9	659.1	655.3
654.3	650.3	698.0	696.3
677.8	680.3	794.1	799.1
806.7	806.3	821.1	820.3
819.6	815.6	828.6	826.3
825.0	826.3	851.4	850.3
838.8	833.3	857.8	858.3
857.8	854.3	894.1	893.9
866.3	869.3	896.7	896.3
892.2	890.3	903.7	905.6
901.1	903.3		

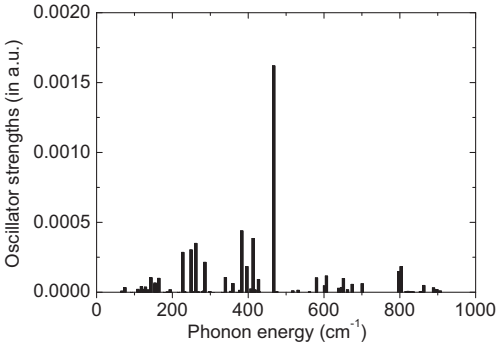

Fig. 4. The calculated oscillator strengths (in a.u., 1 a.u. = 253.2638413 m^3/s^2) for phonons of $SrAl_2O_4$.

Table 4
The calculated dielectric permittivity tensors of $SrAl_2O_4$.

	LDA	GGA
ε_∞	(2.95, 2.98, 2.99)	(2.72, 2.75, 2.76)
ε_0	(8.12, 7.75, 8.51)	(7.92, 7.55, 8.21)

related with the fact that the most intense phonon band is located at 465 cm^{-1} in the Raman spectra [25,30].

3.5. Dielectric properties

The static dielectric permittivity tensor ε_0 was calculated by adding the ionic contributions to the electronic dielectric permittivity tensor ε_∞. In other words, the static dielectric tensor can be decomposed into the contributions of different modes as follows:

$$\varepsilon^0_{\alpha\beta}(\omega) = \varepsilon^\infty_{\alpha\beta} + \sum_m \Delta\varepsilon_{m,\alpha\beta} = \varepsilon^\infty_{\alpha\beta} + \frac{4\pi}{\Omega_0}\sum_m \frac{S_{m,\alpha\beta}}{\omega_m^2} \quad (3)$$

where Ω_0 is the volume of the primitive unit cell, ω_m is the frequency of vibration of normal mode m, and $S_{m,\alpha\beta}$ is the mode oscillator strength, which can be determined by the eigendisplacements and the Born effective charge tensors.

The electronic (ε_∞) and static (ε_0) dielectric permittivity tensors were calculated by both LDA and GGA formalisms, shown in Table 4. However, no experimental data can be found in literature. Thus the present calculations are considered as prediction. The values of dielectric tensors obtained by LDA and GGA are close to each other. The values with LDA are slightly larger than those with GGA. The calculated values in the framework of LDA and GGA are usually overestimated due to their underestimated band gap [31]. Therefore, the experimental values should be predicted to be smaller than those with GGA by several percent. Due to the low symmetry of $SrAl_2O_4$, dielectric permittivity tensors have three independent components. The calculated ε_∞ is nearly isotropic, whereas the calculated ε_0 is anisotropic with about 5% difference. From the present calculations, the ε_0 is much larger than the ε_∞, which indicates that the contributions from the lattice vibrations are dominant since the ε_0 can be decomposed into electronic contributions and ionic contributions.

4. Conclusions

Using DFT and DFPT, the structural, electronic, lattice dynamical, and dielectric properties of $SrAl_2O_4$ were investigated. Both LDA and GGA give the consistent lattice parameters with experimental values [27]. The first pressure derivatives of the bulk modulus are predicted to be 2.5 and 4.3 for LDA and GGA, respectively. The large difference for LDA and GGA results from the high sensitivity for the derivative of pressure. The electronic band structure shows that valence band maximum is comprised of O 2p states and a small amount of Al 3s and 3p states, and the conduction band minimum is comprised of Sr 5s and a small amount of O 2p, Al 3s and Al 3p states. The calculated energy range of phonon frequencies at the center of the Brillouin zone is consistent with the experimental data [30]. It is interesting that the most intense phonon band at 465 cm^{-1} belonging to the bending vibration of the O–Al–O angle in the Raman spectra has the strongest oscillator strength according to the present calculations. The electronic (ε_∞) and static (ε_0) dielectric permittivity tensors are predicted by the calculations with both LDA and GGA formalisms. The prediction shows that the static dielectric permittivity is isotropic and much larger than the electronic dielectric permittivity because the ionic contributions in the static dielectric are dominant.

Acknowledgements

This work was supported by the Innovation Program of Shanghai Municipal Education Commission (Grant No. 11ZZ29), the NSAF of China (Grant No. 10776024), and the NSFC (Grant Nos. 11044011, 10875085, 10904114 and 10974143).

References

[1] C. Liu, Y. Wang, Y. Hu, R. Chen, F. Liao, J. Alloys Compd. 470 (2009) 473.
[2] B. Liu, C. Shi, Z. Qi, Appl. Phys. Lett. 86 (2005) 191111.
[3] B.Y. Geng, J.Z. Ma, F.M. Zhan, J. Alloys Compd. 473 (2009) 530.
[4] L. Xiao, Q. Xiao, Y. Liu, P. Ai, Y. Li, H. Wang, J. Alloys Compd. 495 (2010) 72.
[5] M. Pedroza-Montero, B. Castañeda, M.I. Gil-Tolano, O. Arellano-Tánori, R. Meléndrez, M. Barboza-Flores, Radiat. Meas. 45 (2010) 311.
[6] H. Ryu, K.S. Bartwal, Physica B 404 (2009) 1714.
[7] Y. Xu, D. Ma, M. Guan, X. Chen, Q. Pan, S. Huang, J. Alloys Compd. 502 (2010) 38.
[8] C. Xu, H. Yamada, X. Wang, X. Zheng, Appl. Phys. Lett. 84 (2004) 3040.
[9] H. Yamada, H. Kusaba, C.-N. Xu, Appl. Phys. Lett. 92 (2008) 101909.
[10] M.A. Carpenter, J. Howard, M.J. Andrew, R.E.A. McKnight, Y. Liu, R.L. Withers, J. Appl. Phys. 107 (2010) 013505.
[11] Z. Fu, S. Zhou, T. Pan, S. Zhang, J. Solid State Chem. 178 (2005) 230.
[12] H. Yamada, C.-N. Xu, J. Appl. Phys. 102 (2007) 126103.
[13] J. Hölsä, T. Laamanen, M. Lastusaari, J. Niittykoski, P. Novák, J. Rare Earths 27 (2009) 550.
[14] K.S. Bartwal, H. Ryu, M.G. Brik, I. Sildos, Opt. Mater. 32 (2010) 1329.
[15] The ABINIT code is a common project of the Université Catholique de Louvain, and other contributors (URL http://www.abinit.org).
[16] X. Gonze, J.M. Beuken, R. Caracas, F. Detraux, M. Fuchs, G.M. Rignanese, L. Sindic, M. Verstraete, G. Zerah, F. Jollet, M. Torrent, A. Roy, M. Mikami, P. Ghosez, J.Y. Raty, D.C. Allan, Comp. Mater. Sci. 25 (2002) 478.
[17] P. Hohenberg, W. Kohn, Phys. Rev. 136 (1964) B864.
[18] W. Kohn, L.J. Sham, Phys. Rev. 140 (1964) A1133.
[19] D.M. Ceperley, B.J. Alder, Phys. Rev. Lett. 45 (1980) 566.
[20] J.P. Perdew, K. Burke, M. Ernzerhof, Phys. Rev. Lett. 77 (1996) 3865.
[21] H.B. Schlegel, J. Comput. Chem. 3 (1982) 214.
[22] X. Gonze, Phys. Rev. B 55 (1997) 10337.
[23] X. Gonze, D.C. Allan, M.P. Teter, Phys. Rev. Lett. 68 (1992) 3603.
[24] H.J. Monkhorst, J.D. Pack, Phys. Rev. B 13 (1976) 5188.
[25] E. Cordoncillo, B. Julian-Lopez, M. Martínez, M.L. Sanjuán, P. Escribano, J. Alloys Compd. 484 (2009) 693.
[26] F. Birch, Phys. Rev. 71 (1947) 809.
[27] A.R. Schulze, H. Mueller-Buschbaum, Z. Anorg. Allg. Chem. 475 (1981) 205.
[28] M. Nanko, S. Taniguchi, K. Matsumaru, Adv. Tech. Mat. Mat. Proc. J. 9 (2007) 125.
[29] D. Jia, D.N. Hunter, J. Appl. Phys. 100 (2006) 113125.
[30] P. Escribano, M. Marchal, M.L. Sanjuan, P. Alonso-Gutierrezb, B. Julian, E. Cordoncillo, J. Solid State Chem. 178 (2005) 1978.
[31] G.M. Rignanese, F. Detraux, A. Pasquarello, Phys. Rev. B 63 (2001) 104305.